Two-channel anomalous Hall effect in math xmlns="http://www.w3.org/1998/Math/MathML">msub>mi >SrRuO/mi>mn>3/mn>/msub>/math>

Graham Kimbell, Paul M. Sass, Bart Woltjes, Eun Kyo Ko, Tae Won Noh, Weida Wu, and Jason W. A. Robinson

Phys. Rev. Materials **4**, 054414 — Published 18 May 2020

DOI: 10.1103/PhysRevMaterials.4.054414

Two-channel anomalous Hall effect in $SrRuO_3$

Graham Kimbell,[1] Paul M. Sass,[2] Bart Woltjes,[1] Eun Kyo Ko,[3,4] Tae Won Noh,[3,4] Weida Wu,[2] and Jason W. A. Robinson[1,*]

[1]*Department of Materials Science & Metallurgy, University of Cambridge, CB3 0FS, United Kingdom*
[2]*Department of Physics & Astronomy, Rutgers University, Piscataway, NJ 08854, USA*
[3]*Center for Correlated Electron Systems, Institute for Basic Science (IBS), Seoul 08826, Republic of Korea*
[4]*Department of Physics & Astronomy, Seoul National University, Seoul 08826, Republic of Korea*

(Dated: April 13, 2020)

The Hall effect in $SrRuO_3$ thin-films near the thickness limit for ferromagnetism shows an extra peak in addition to the ordinary and anomalous Hall effects. This extra peak has been attributed to a topological Hall effect due to two-dimensional skyrmions in the film around the coercive field; however, the sign of the anomalous Hall effect in $SrRuO_3$ can change as a function of saturation magnetization. Here we report Hall peaks in $SrRuO_3$ in which volumetric magnetometry measurements and magnetic force microscopy indicate that the peaks result from the superposition of two anomalous Hall channels with opposite sign. These channels likely form due to thickness variations in $SrRuO_3$, creating two spatially separated magnetic regions with different saturation magnetizations and coercive fields. The results are central to the development of strongly correlated materials for spintronics.

I. INTRODUCTION

In the Hall effect a transverse electric field (E_x) is generated under an applied longitudinal current density (J_y). In conventional tensor notation, $E_x = \rho_{xy} J_y$ where ρ_{xy} is the Hall resistivity. In a ferromagnet, $\rho_{xy} = R_0 H_z + R_s M_z$, the ordinary Hall effect (OHE) coefficient (R_0) is proportional to the out-of-plane applied magnetic field (H_z), is caused by the Lorentz force, and its sign follows the sign of the charge carriers; the anomalous Hall effect (AHE) coefficient (R_s) is proportional to the out-of-plane component of magnetization (M_z). Recently, there have been reports of an additional peak in the Hall resistivity (illustrated in Fig. 1(a)) in ultrathin films of ferromagnetic $SrRuO_3$ [1–21]. This additional peak is sometimes attributed to a spin texture with net spin chirality [1–11], which results in electrons experiencing an effective magnetic field from the accumulation of a Berry phase in real space. This additional contribution to the Hall effect is called the topological Hall effect (THE) [22] (Fig. 1(b)). A possible source of chirality is skyrmions in the $SrRuO_3$, which are topologically protected magnetic textures. Skyrmions can be stabilized through a competition between the ferromagnetic exchange and the Dzyaloshinkii-Moria interaction (DMI) resulting from the combination of spin-orbit coupling and broken inversion symmetry. The source of spin-orbit coupling is either extrinsic from a heavy-metal oxide layer such as $SrIrO_3$ [1–3], or intrinsic to the $SrRuO_3$ [4–8]. The broken inversion symmetry arises from the interfaces between $SrRuO_3$ and adjacent layers. It is also possible that the DMI is sufficient that domain walls around bubble domains have net chirality and therefore give a THE contribution [23].

Alternatively, the peak in the Hall effect could arise due to the superposition of two AHEs with different signs [13–21, 24, 25] (Fig. 1(c)). The AHE in $SrRuO_3$ has a non-monotonic temperature and resistivity dependence which cannot be explained by scattering mechanisms alone [26–28], instead, it is thought to also depend on the Berry curvature in k-space [29–32]. This is an intrinsic mechanism for the Hall effect and should not be confused with the extrinsic accumulation of Berry phase in real space by skyrmions. The anomalous Hall coefficient in $SrRuO_3$ is sensitively dependent on the band structure and magnetization [29, 30], and is thus dependent on temperature (T) and thickness, as well as strain, disorder and stoichiometry. Crucially, the AHE in $SrRuO_3$ undergoes a sign-change as a function of saturation magnetization [33–35]. Therefore, if the $SrRuO_3$ is inhomogeneous, consisting of two magnetic regions with different coercive fields and saturation magnetizations giving opposite sign AHEs, a peak will necessarily appear in the Hall effect.

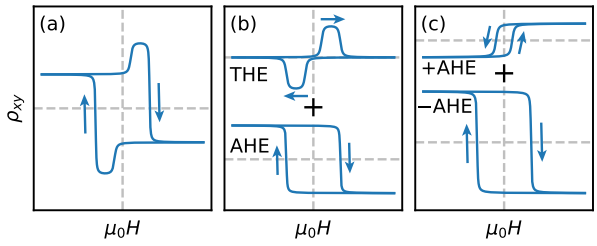

FIG. 1. (a) Illustrations of the peak structure in the Hall effect describing how the peaks may arise due to (b) the superposition of the AHE and THE, or (c) two AHE channels with different signs and coercive fields.

In this paper, we show that the additional peak in the $SrRuO_3$ Hall effect is likely caused by the superposition of two opposite sign AHEs from two magnetic regions with different saturation magnetizations. We argue that these two regions arise from single unit-cell thickness variations in $SrRuO_3$ films that are close to the thickness limit for ferromagnetism. $SrRuO_3$ films between 4 and 5 pseudocubic unit cells (UC) thick reproducibly display additional peaks in Hall effect measurements. Volumetric magnetometry shows two magnetic transition temperatures and two switching fields consistent with the Hall effect, and magnetic force microscopy (MFM) confirms these two regions are spatially separated and magnetically non-uniform.

* jjr33@cam.ac.uk

II. METHODS

$SrRuO_3$ films are grown by pulsed laser deposition on TiO_2-terminated (001)-oriented $SrTiO_3$. The $SrTiO_3$ is held at 600°C during deposition under a flow of 100 mTorr O_2, then cooled in 400 mTorr O_2 at -5°C min^{-1}. Laser pulses of 10 Hz with an energy density ≈ 2.5 J cm^{-2} give a growth rate of one UC ($c = 3.95$ Å) per 10 seconds. $SrRuO_3$ grows initially layer-by-layer then transitions to step-flow-growth after several UCs [36]. In the first layer, the substrate changes from B-site (TiO_2) to A-site (SrO) termination [37]. This can be considered as half-integer UC thicknesses of $SrRuO_3$, or as the first half UC being a continuation of the $SrTiO_3$ substrate; the latter definition is used here, as depicted in Fig. 2(c). The growth rate (and substrate terrace width) is high enough to reduce growth instabilities caused by the strain in $SrRuO_3$ [38], but low enough to allow for diffusion of adatoms across terraces [39]. TiO_2-terminated $SrTiO_3$ ensures uniform nucleation and growth of $SrRuO_3$ [40].

The structural quality of films is assessed by X-ray diffraction (XRD), X-ray reflectivity (XRR), and atomic force microscopy (AFM). The growth rate is calibrated by fitting fringes in XRR and XRD for thicker samples (see Supplementary Information [41]).

Volumetric magnetic properties are investigated using a superconducting quantum interference device with films loaded out-of-plane with respect to the applied magnetic field. To identify background signals, measurements were taken of both films, as-received substrates, and substrates which underwent the same growth and cleaning conditions as the film without any material deposited (see Supplementary Information [41]).

Transport measurements are made using unpatterned van der Pauw geometries. The transverse resistance data is antisymmetrised to separate the Hall effect from the longitudinal component of resistance (see Supplementary Information [41]).

Micromagnetic surface measurements are carried out using a cryogenic MFM with piezoresistive cantilevers, recorded in constant height mode with the scanning plane 100 nm above the $SrRuO_3$ film surface. For further details see [42].

III. RESULTS & DISCUSSION

$SrRuO_3$ films are epitaxial and fully strained to the $SrTiO_3$ substrate (see Supplementary Information [41]). Fig. 2(a) shows an AFM image of a 4.5 UC thick film with an atomically flat surface and a step-and-terrace structure. A line profile (Fig. 2(b)) shows the steps are one UC in height ($c = 3.95$ Å), indicating a single surface termination in the $SrRuO_3$. Strain-induced growth instabilities in $SrRuO_3$ usually manifest as curvature at step edges.

Electronic transport of a 10 nm thick $SrRuO_3$ film (Figs. 3(a) and 3(b)) show a spontaneous Hall resistance ($R_{xy,s}$) attributed to the AHE, which changes sign from positive (+ve) at high T to negative (−ve) at low T. This unusual $T-$dependence has been observed previously [30, 34] and is

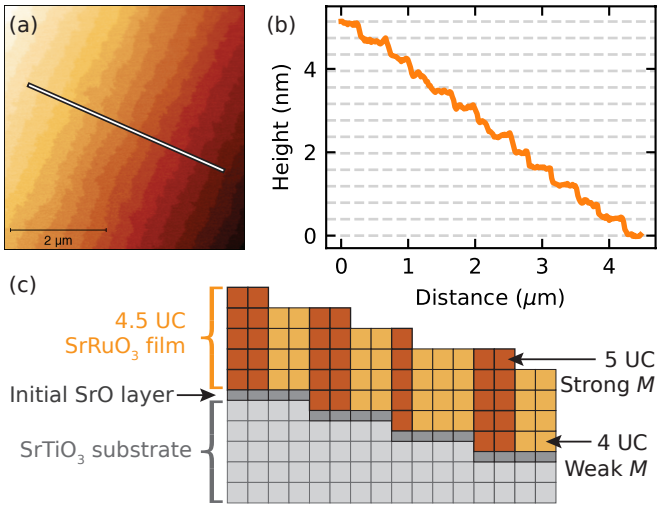

FIG. 2. (a) Plane-leveled AFM image of a 4.5 UC thick $SrRuO_3$ film, showing a step and terrace structure typical of step-flow growth. (b) The corresponding height profile along the line drawn in (a), the horizontal dotted lines are separations of one UC ($c = 3.95$ nm, as measured in XRD on thicker films). (c) Illustration of thickness variations in the film.

related to the intrinsic nature of the AHE in $SrRuO_3$. We note that the apparent two magnetic switches seen in this case are likely caused by the rotation of the easy axis in $SrRuO_3$ away from the out-of-plane direction with increasing thickness, and not by two magnetic regions [43]. The spontaneous volume magnetization (M_s) of a film is used as a scaling parameter for the AHE, so the magnetization of the 10 nm film is measured versus T (Fig. 3(c)), showing only one transition at the Curie temperature ($T_C \approx 144$ K). The spontaneous Hall resistivity ($\rho_{xy,s}$) and conductivity (estimated as $\sigma_{xy,s} \approx -\rho_{xy,s}/\rho_{xx}^2$ where ρ_{xx} is the longitudinal resistivity) are plotted in Figs. 3(d) and 3(e). The Hall conductivity as a function of magnetization agrees well with literature values [30] despite differences in material properties. The anomalous Hall resistivity switches from +ve at low M_s, to −ve at high M_s.

Hall measurements of a 4.5 UC thick film shows additional peaks in R_{xy}, similar to those attributed to a THE. Fig. 4(a) shows the $T-$dependence of $R_{xy}(H)$, with peaks below 90 K; these data are fitted assuming the two-channel AHE model, and Fig. 4(b) is the same data at only 10 K. The data is well reproduced by these two AHEs (Fig. 4(c)). The spontaneous anomalous Hall resistances of the two channels extracted from the fit is shown as a function of T in Fig. 4(f). The $T-$dependence of the two AHE channels can be compared to that of the thicker film (Fig. 3(b)): a similar $T-$dependence is seen but suppressed to lower T slightly in AHE_2, and suppressed significantly in AHE_1.

An $M(H)$ loop at 10 K is shown in Fig. 4(d) (for full temperature range see Supplementary Information [41]). This is fitted using the same function as for the anomalous Hall effect, where only the scaling of the two components are varied as free parameters; these two components are shown in Fig. 4(e). There are two clear switches in the magnetometry

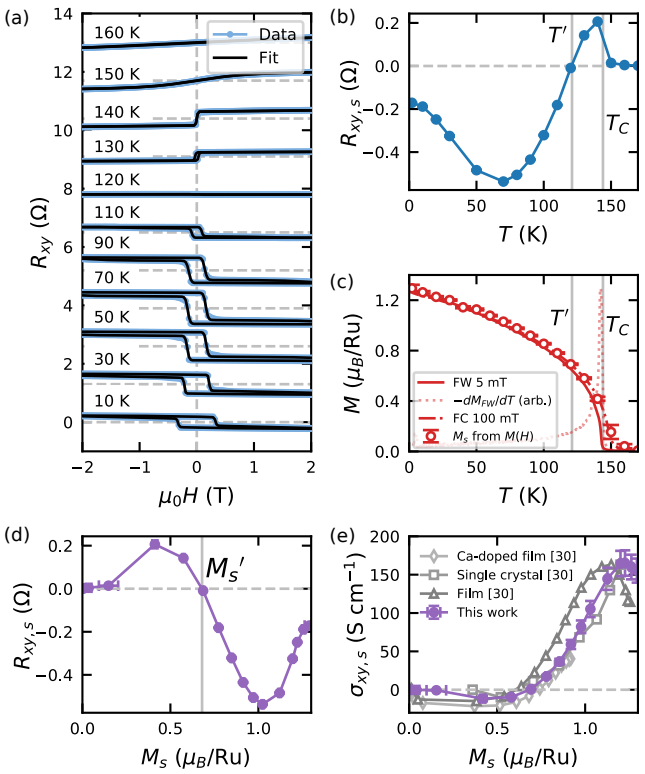

FIG. 3. Transport and magnetometry of a 10 nm thick film. (a) $R_{xy}(H)$ at different T. The OHE is removed by a linear fitting at high field (5-6 T). (b) The spontaneous anomalous Hall effect extracted from (a) as a function of temperature. This is non-monotonic with a sign change at $T' \approx 121$ K. (c) Magnetization as a function of temperature. Field cool and field warming curves have substrate curves subtracted and are shifted vertically so $M(170) = 0$, the dotted curve shows the derivative of the 5 mT field warm curve with arbitrary units to highlight the magnetic transition. Points from $M(H)$ curves are spontaneous magnetization taken as average moment under 1 T for saturated quadrants. There is no magnetic transition evident at the AHE sign-change. (d) Spontaneous anomalous Hall resistivity of the $SrRuO_3$ as a function of spontaneous magnetization. The anomalous Hall effect is +ve for small M_s, and −ve for large M_s, switching at $M_s' \approx 0.7$ μ_B/Ru. (e) Spontaneous anomalous Hall conductivity as a function of spontaneous magnetization, compared to previous literature values [30].

which correspond to the two switches in Hall effect, and the smaller magnetic switch gives a +ve AHE component, whilst the larger switch gives a −ve AHE, as expected.

The magnetization versus temperature is shown in Fig. 4(g); there appears to be two separate magnetic transitions which is most obvious in the remanence curve (saturating with 7 T and warming in a 5 mT field, solid curve) and its derivative (dotted curve, arbitrary units and flipped for clarity), which show two transitions at $T_{C1} \approx 77$ K and $T_{C2} \approx 115$ K, labeled on the graph with solid gray lines. These two transition temperatures are also plotted in Fig. 4(f) and agree with the appearance of the spontaneous components of each AHE channel, so we attribute these transitions to the Curie temperatures for the two magnetic regions. It is likely that the 4 UC regions correspond to the lower T_C, lower H_c and +ve AHE, whilst the 5 UC regions correspond to the higher T_C, higher H_c and −ve AHE (at low T).

A $SrRuO_3$ film prepared in a different system and measured sooner after deposition also shows two switches in $R_{xy}(H)$ (Fig. 5(a)), $R_{xy}(H)$ (Fig. 5(f)), $M(H)$, and $M(T)$ (see Supplementary Information [41]). However, the Hall effect transitions from a peak-like structure at high T (one low M_s +ve AHE region, one high M_s −ve AHE region, Figs. 5(b) and 5(c)) to a step-like structure at low T (two high M_s −ve AHE regions, Figs. 5(d) and 5(e)). This step-like structure is consistent with two AHEs. To explain this in terms of the THE, the OHE or spin polarisation of the $SrRuO_3$ would change sign at ≈ 53 K. An OHE sign change at this T is not observed here (Fig. 5(g)), but we note that though generally assumed to be constant below TC, the temperature dependent spin-polarisation of SrRuO3 is not well characterized theoretically or experimentally. An alternative explanation might be that the THE peak is shifting to higher fields above the coercive field of $SrRuO_3$.This is, however, unlikely since an intermediate peak plus step shape is expected in this case.

MFM images show stripe domains in the $SrRuO_3$ films consisting of two regions with different H_c and magnetic strengths. Figs. 6(a)-6(e) are MFM images at 10 K, 0.1 T after saturating at −ve field and sequentially applying different fields, which are also shown on the $R_{xy}(H)$ loop in Fig. 6(f). Following the increasing field: at 0.2 T the film is still negatively magnetized, stripe contrast is present as thinner regions have a lower M_s; 0.4 T, weaker regions (yellow-green) are switching; 0.9 T, weaker regions are now positively magnetized (light blue), this switch corresponds to H_{c1} for the +ve AHE component (AHE_1); 1.3 T, stronger magnetic regions (red) begin to switch (blue); 1.6 T, all strong regions have switched to +ve magnetization (blue), this corresponds to H_{c2} for the −ve AHE component (AHE_2). The stripe contrast remains even at high field due to the difference in M_s between the two regions.

The root mean square (RMS) deviation of the MFM signal is also plotted in Fig. 6(f) (green squares). This quantifies the magnetic inhomogeneity in the film - this peak in RMS signal matches well with the peak in the Hall effect.

Fig. 6(g) shows the change in MFM signal through the first switch, and Fig. 6(h) through the second switch - each switch corresponds to one set of stripes changing magnetization. The combination of these two images is shown in Fig. 6(i), the lack of overlap demonstrating that the two switches correspond to two spatially separated magnetic regions.

These data are consistent with the picture that one UC thickness variations across terrace steps create two magnetic regions with different M_s, which results in two AHE channels with different signs and, due to their differing H_c, a peak appears in the Hall effect.

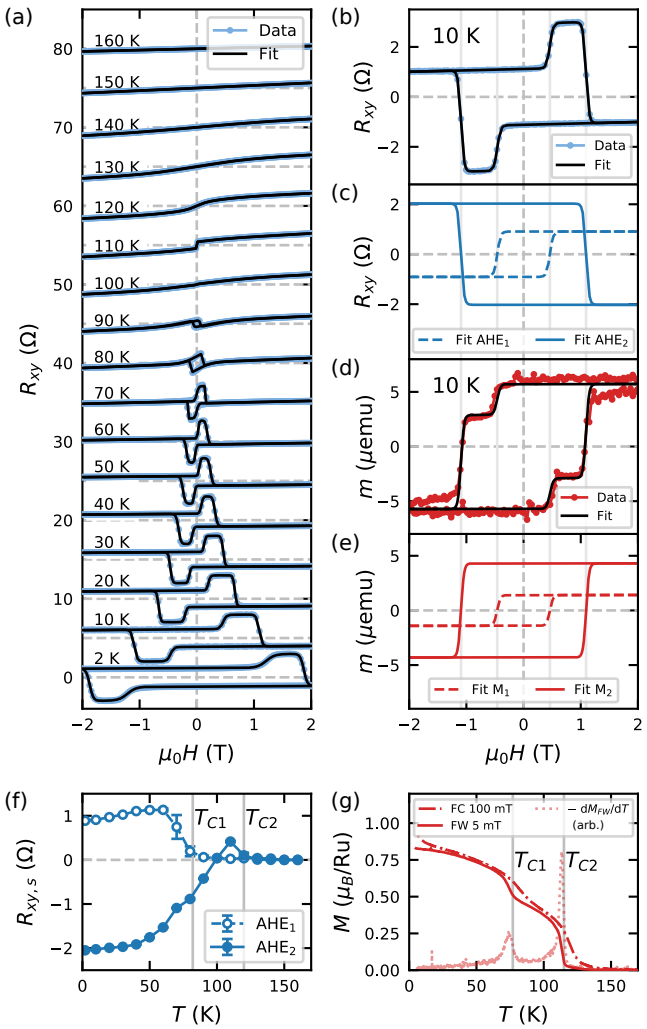

FIG. 4. Transport and magnetometry of a 4.5 UC thick $SrRuO_3$ film. (a) $R_{xy}(H)$ at different T. The data (blue points) are fitted to a function of two sigmoids as an approximation of two AHEs (black line). (b) $R_{xy}(H)$ of the film at 10 K, the black line is the two AHE fit. (c) The two fit components from from (b). (d) Moment (m) versus H of the film at 10 K, showing two switches at the same coercive fields as in the Hall resistance. For the fit, the widths and coercive fields from (b,c) are fixed, and the scalings are fit parameters. (e) The two fit components from (d). (f) $T-$dependence of the spontaneous anomalous Hall resistance of the two channels, defined as the mean and standard deviation of anomalous Hall resistance in the $0-100$ mT range of the saturated quadrant of an individual fit component. (g) $T-$dependence of the magnetization in field cooling (FC) in 100 mT, and field warming (FW) in 5 mT after saturating at 7 T. Data have substrate curves subtracted and are shifted vertically so $M(170) = 0$. The dotted curve shows the derivative of the 5 mT field warm curve with arbitrary units to highlight the two magnetic transitions.

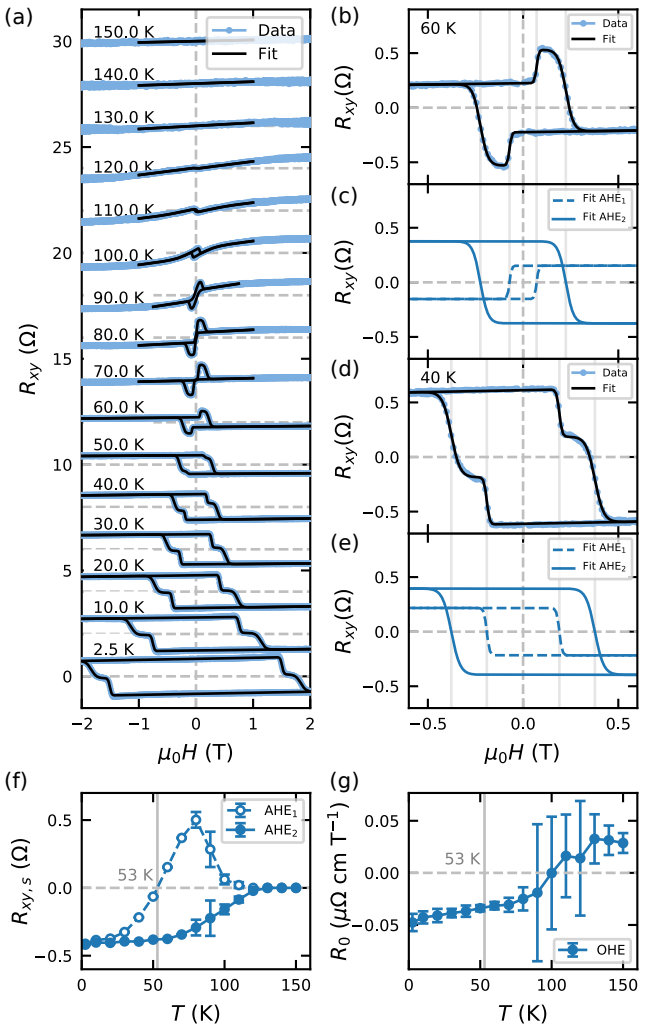

FIG. 5. Transport measurements of a nominally 4.0 UC thick $SrRuO_3$ film. (a) $T-$dependence of $R_{xy}(H)$, showing a transition from the usual 'peak' shape below T_C, to a 'step' shape at 50 K and below. (b) $R_{xy}(H)$ at 60 K showing the usual 'peak' shape, with the fitting shown in black. (c) The two components of the fit at 60 K: one $+$ve and one $-$ve AHE. (d) $R_{xy}(H)$ at 40 K showing the 'step' shape, with the fitting shown in black. (e) The two components of the fit at 40 K: two $-$ve AHEs. (f) $T-$dependence of the two AHE components. One component experiences a sign change near 53 K, where the anomalous Hall signal changes from step-like at low T to peak-like at high T. (g) $T-$dependence of the OHE, found from a linear fit at 2-3 T, the error is the difference between the OHE estimated by a high field and low field fits. The error becomes very large above 90 K, where it becomes difficult to separate the broad paramagnetic AHE from the OHE. The OHE does not change sign near 53 K.

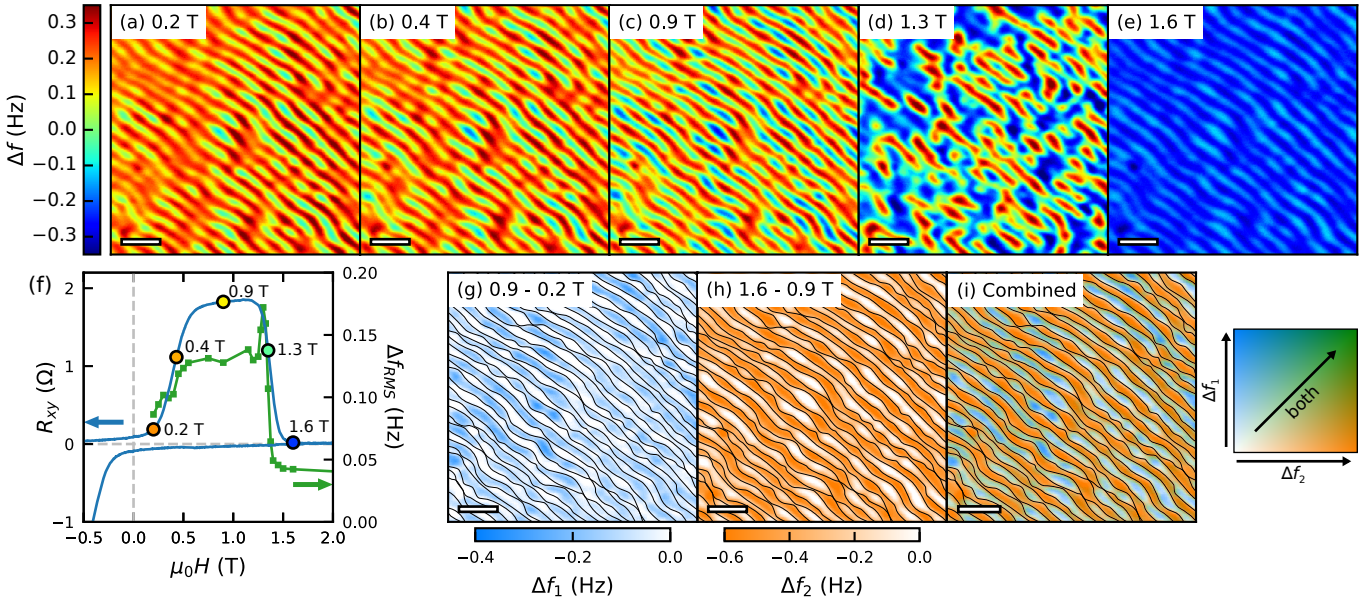

FIG. 6. MFM images at 10 K, 0.1 T after applying different fields. Scale bars are 1 μm. Δf, the change in resonant frequency, is proportional to out-of-plane stray field gradient. The sign of Δf is opposite to the sign of magnetization. Images (a)-(e) show the progression of the magnetic structure of the film through the two transitions. Red/yellow is negatively magnetized, blue/cyan is positively magnetized. (f) shows the anomalous Hall resistance (blue line) of the film as a function of field, with points labeled where the presented MFM images were measured. The RMS deviation of the MFM signal (green squares) shows a peak in inhomogeneity corresponding to the peak in the Hall effect. (g) The change in MFM signal through the first transition, showing only one set of stripes switching. Black lines are added as a guide to the eye. (h) The change in MFM signal through the second transition, showing the other set of stripes switching. The same black lines are a guide to the eye. (i) The images from (g) and (h) combined additively. The MFM signal either changes in the first transition or the second rather than both, meaning there are two spatially magnetic regions with two different coercive fields.

IV. CONCLUSION

The anomalous Hall coefficient in $SrRuO_3$ depends strongly on the band structure and magnetization, and can switch sign with parameters that affect these, such as temperature, film thickness, or disorder. In a $SrRuO_3$ thin film, if there are two magnetic regions with different coercive fields and signs of the AHE, then peaks will appear in Hall effect measurements. Here, 4 to 5 UC thick $SrRuO_3$ films show peaks in the Hall effect, similar peaks have been observed previously and are sometimes attributed to a THE caused by magnetic skyrmions. $SrRuO_3$ films in this work show two spatially separated magnetic regions with different T_C, M_s and H_c values. The stripe pattern of these two regions indicate they likely result from step-flow growth giving single unit cell thickness variations in the film across terrace steps. These two magnetic regions can explain the peaks in the Hall effect by the superposition of two AHEs with different signs. Additionally, a film showed a smooth transition from peak-like to step-like Hall effect, which is not easily explained by a THE.

These data do not exclude the existence of a THE, however we show that the observation of a peak in the Hall effect does not give unambiguous evidence for a THE caused by magnetic skyrmions, particularly in the case where the magnetic structure of the $SrRuO_3$ film is inhomogenously modified.

ACKNOWLEDGMENTS

This work is supported by the EPSRC through the Core-to-Core International Network "Oxide Superspin" (EP/P026311/1) and the Doctoral Training Partnership Grant (EP/N509620/1). Additional support from the Office of Basic Energy Sciences Division of Materials Sciences and Engineering, US Department of Energy under Award numbers DE-SC0018153, and the Research Center Program of IBS (Institute for Basic Science) in Korea (IBS-R009-D1).

[1] J. Matsuno, N. Ogawa, K. Yasuda, F. Kagawa, W. Koshibae, N. Nagaosa, Y. Tokura, and M. Kawasaki, Interface-driven topological Hall effect in $SrRuO_3$-$SrIrO_3$ bilayer, Science Advances **2**, e1600304 (2016).

[2] Y. Ohuchi, J. Matsuno, N. Ogawa, Y. Kozuka, M. Uchida, Y. Tokura, and M. Kawasaki, Electric-field control of anomalous and topological Hall effects in oxide bilayer thin films, Nature Communications **9**, 213 (2018).

[3] K.-Y. Meng, A. S. Ahmed, M. Baani, A.-O. Mandru, X. Zhao, N. Bagus, B. D. Esser, J. Flores, D. W. McComb, H. J. Hug, and F. Yang, Observation of Nanoscale Skyrmions in $SrIrO_3$/$SrRuO_3$ Bilayers, Nano Letters **19**, 3169 (2019).

[4] B. Sohn, B. Kim, S. Y. Park, H. Y. Choi, J. Y. Moon, T. Choi, Y. J. Choi, T. W. Noh, H. Zhou, S. H. Chang, J. H. Han, and C. Kim, Emergence of robust 2D skyrmions in $SrRuO_3$ ultrathin film without the capping layer, arXiv:1810.01615 [cond-mat] (2018).

[5] Y. Gu, Y.-W. Wei, K. Xu, H. Zhang, F. Wang, F. Li, M. S. Saleem, C.-Z. Chang, J. Sun, C. Song, J. Feng, X. Zhong, W. Liu, Z. Zhang, J. Zhu, and F. Pan, Interfacial oxygen-octahedral-tilting-driven electrically tunable topological Hall effect in ultrathin $SrRuO_3$ films, Journal of Physics D: Applied Physics **52**, 404001 (2019).

[6] Q. Qin, L. Liu, W. Lin, X. Shu, Q. Xie, Z. Lim, C. Li, S. He, G. M. Chow, and J. Chen, Emergence of Topological Hall Effect in a $SrRuO_3$ Single Layer, Advanced Materials **31**, 1807008 (2019).

[7] B. Sohn, B. Kim, J. W. Choi, S. H. Chang, J. H. Han, and C. Kim, Hump-like structure in Hall signal from ultra-thin $SrRuO_3$ films without inhomogeneous anomalous Hall effect, Current Applied Physics **20**, 186 (2020).

[8] P. Zhang, A. Das, E. Barts, M. Azhar, L. Si, K. Held, M. Mostovoy, and T. Banerjee, Robust skyrmion-bubble textures in $SrRuO_3$ thin films stabilized by magnetic anisotropy, arXiv:2001.07039 [cond-mat] (2020).

[9] L. Wang, Q. Feng, Y. Kim, R. Kim, K. H. Lee, S. D. Pollard, Y. J. Shin, H. Zhou, W. Peng, D. Lee, W. Meng, H. Yang, J. H. Han, M. Kim, Q. Lu, and T. W. Noh, Ferroelectrically tunable magnetic skyrmions in ultrathin oxide heterostructures, Nature Materials **17**, 1087 (2018).

[10] W. Wang, M. W. Daniels, Z. Liao, Y. Zhao, J. Wang, G. Koster, G. Rijnders, C.-Z. Chang, D. Xiao, and W. Wu, Spin chirality fluctuation in two-dimensional ferromagnets with perpendicular magnetic anisotropy, Nature Materials **18**, 1054 (2019).

[11] Z. Li, S. Shen, Z. Tian, K. Hwangbo, M. Wang, Y. Wang, F. M. Bartram, L. He, Y. Lyu, Y. Dong, G. Wan, H. Li, N. Lu, J. Zang, H. Zhou, E. Arenholz, Q. He, L. Yang, W. Luo, and P. Yu, Reversible manipulation of the magnetic state in $SrRuO_3$ through electric-field controlled proton evolution, Nature Communications **11**, 184 (2020).

[12] Y. Gu, C. Song, Q. Zhang, F. Li, H. Tan, K. Xu, J. Li, M. S. Saleem, M. U. Fayaz, J. Peng, F.-X. Hu, L. Gu, W. Liu, Z. Zhang, and F. Pan, Interfacial Control of Ferromagnetism in Ultrathin $SrRuO_3$ Films Sandwiched between Ferroelectric $BaTiO_3$ Layers, ACS Applied Materials & Interfaces **12**, 6707 (2020).

[13] D. J. Groenendijk, C. Autieri, T. C. van Thiel, W. Brzezicki, N. Gauquelin, P. Barone, K. H. W. v. d. Bos, S. van Aert, J. Verbeeck, A. Filippetti, S. Picozzi, M. Cuoco, and A. D. Caviglia, Berry phase engineering at oxide interfaces, arXiv:1810.05619 [cond-mat] (2018).

[14] D. Kan, T. Moriyama, K. Kobayashi, and Y. Shimakawa, Alternative to the topological interpretation of the transverse resistivity anomalies in $SrRuO_3$, Physical Review B **98**, 180408(R) (2018).

[15] G. Malsch, D. Ivaneyko, P. Milde, L. Wysocki, L. Yang, P. H. M. van Loosdrecht, I. Lindfors-Vrejoiu, and L. M. Eng, Correlating the nanoscale structural, magnetic and magneto-transport properties in $SrRuO_3$-based perovskite oxide ultra-thin films, arXiv:1910.01474 [physics.app-ph] (2019).

[16] Z. Y. Ren, Z. Yuan, L. F. Wang, F. Shao, P. F. Liu, J. Teng, K. K. Meng, X. G. Xu, J. Miao, and Y. Jiang, Nonvolatile ferroelectric field control of the anomalous Hall effect in $BiFeO_3/SrRuO_3$ bilayer, arXiv:1910.02588 [cond-mat.str-el] (2019).

[17] L. Wang, Q. Feng, H. G. Lee, E. K. Ko, Q. Lu, and T. W. Noh, Controllable thickness inhomogeneity and Berry-curvature-engineering of anomalous Hall effect in $SrRuO_3$ ultrathin films, arXiv:1908.08211 [cond-mat] (2019).

[18] L. Wu, F. Wen, Y. Fu, J. H. Wilson, X. Liu, Y. Zhang, D. M. Vasiukov, M. S. Kareev, J. H. Pixley, and J. Chakhalian, Berry phase manipulation in ultrathin $SrRuO_3$ films, arXiv:1907.07579 [cond-mat] (2019).

[19] M. Ziese, L. Jin, and I. Lindfors-Vrejoiu, Unconventional anomalous Hall effect driven by oxygen-octahedra-tailoring of the $SrRuO_3$ structure, Journal of Physics: Materials **2**, 034008 (2019).

[20] P.-C. Wu, H. Song, Y. Yuan, B. Feng, Y. Ikuhara, R. Huang, P. Yu, C.-G. Duan, and Y.-H. Chu, Thickness dependence of transport behaviors in $SrRuO_3/SrTiO_3$ superlattices, Physical Review Materials **4**, 014401 (2020).

[21] D. Kan, T. Moriyama, and Y. Shimakawa, Field-sweep-rate and time dependence of transverse resistivity anomalies in ultrathin $SrRuO_3$ films, Physical Review B **101**, 014448 (2020).

[22] P. Bruno, V. K. Dugaev, and M. Taillefumier, Topological Hall Effect and Berry Phase in Magnetic Nanostructures, Physical Review Letters **93**, 096806 (2004).

[23] J. Jiang, D. Xiao, F. Wang, J.-H. Shin, D. Andreoli, J. Zhang, R. Xiao, Y.-F. Zhao, M. Kayyalha, L. Zhang, K. Wang, J. Zang, C. Liu, N. Samarth, M. H. W. Chan, and C.-Z. Chang, Crossover of Quantum Anomalous Hall to Topological Hall Effect in Magnetic Topological Insulator Sandwich Heterostructures, arXiv:1901.07611 [cond-mat] (2019).

[24] A. Gerber, Interpretation of experimental evidence of the topological Hall effect, Physical Review B **98**, 214440 (2018).

[25] L. Wu and Y. Zhang, Artificial Topological Hall Effect Induced by Intrinsic Thickness Non-uniformity in Ultrathin $SrRuO_3$ Films, arXiv:1812.09847 [cond-mat.mtrl-sci] (2018).

[26] L. Berger, Side-Jump Mechanism for the Hall Effect of Ferromagnets, Physical Review B **2**, 4559 (1970).

[27] J. Smit, The spontaneous hall effect in ferromagnetics I, Physica **21**, 877 (1955).

[28] J. Smit, The spontaneous hall effect in ferromagnetics II, Physica **24**, 39 (1958).

[29] M. Onoda and N. Nagaosa, Topological Nature of Anomalous Hall Effect in Ferromagnets, Journal of the Physical Society of Japan **71**, 19 (2002).

[30] Z. Fang, N. Nagaosa, K. S. Takahashi, A. Asamitsu, R. Mathieu, T. Ogasawara, H. Yamada, M. Kawasaki, Y. Tokura, and K. Terakura, The Anomalous Hall Effect and Magnetic Monopoles in Momentum Space, Science **302**, 92 (2003).

[31] T. Jungwirth, Q. Niu, and A. H. MacDonald, Anomalous Hall Effect in Ferromagnetic Semiconductors, Physical Review Letters **88**, 207208 (2002).

[32] N. Haham, Y. Shperber, M. Schultz, N. Naftalis, E. Shimshoni, J. W. Reiner, and L. Klein, Scaling of the anomalous Hall effect in $SrRuO_3$, Physical Review B **84**, 174439 (2011).

[33] R. Mathieu, A. Asamitsu, H. Yamada, K. S. Takahashi, M. Kawasaki, Z. Fang, N. Nagaosa, and Y. Tokura, Scaling of the Anomalous Hall Effect in $Sr_{1-x}Ca_xRuO_3$, Physical Review Letters **93**, 016602 (2004).

[34] L. Klein, J. R. Reiner, T. H. Geballe, M. R. Beasley, and A. Kapitulnik, Extraordinary Hall effect in $SrRuO_3$, Physical Review B **61**, R7842 (2000).

[35] M. Izumi, K. Nakazawa, Y. Bando, Y. Yoneda, and H. Terauchi, Magnetotransport of $SrRuO_3$ Thin Film on $SrTiO_3$(001), Journal of the Physical Society of Japan **66**, 3893 (1997).

[36] J. Choi, C. B. Eom, G. Rijnders, H. Rogalla, and D. H. A. Blank, Growth mode transition from layer by layer to step flow during the growth of heteroepitaxial $SrRuO_3$ on (001) $SrTiO_3$, Applied Physics Letters **79**, 1447 (2001).

[37] G. Rijnders, D. H. A. Blank, J. Choi, and C.-B. Eom, Enhanced surface diffusion through termination conversion during epitaxial $SrRuO_3$ growth, Applied Physics Letters **84**, 505 (2004).

[38] D. Estve, T. Maroutian, V. Pillard, and P. Lecoeur, Step velocity tuning of $SrRuO_3$ step flow growth on $SrTiO_3$, Physical Review B **83**, 193401 (2011).

[39] R. A. Rao, Q. Gan, and C. B. Eom, Growth mechanisms of epitaxial metallic oxide $SrRuO_3$ thin films studied by scanning tunneling microscopy, Applied Physics Letters **71**, 1171 (1997).

[40] R. Bachelet, F. Snchez, J. Santiso, C. Munuera, C. Ocal, and J. Fontcuberta, Self-Assembly of $SrTiO_3$ (001) Chemical-Terminations: A Route for Oxide-Nanostructure Fabrication by Selective Growth, Chemistry of Materials **21**, 2494 (2009).

[41] See Supplemental Material at [URL will be inserted by publisher] for additional details and characterization of samples.

[42] P. M. Sass, W. Ge, J. Yan, D. Obeysekera, J. J. Yang, and W. Wu, Magnetic imaging of antiferromagnetic domain walls, arXiv:1910.06488 [cond-mat.mtrl-sci] , 14 (2019).

[43] M. Schultz, S. Levy, J. W. Reiner, and L. Klein, Magnetic and transport properties of epitaxial films of $SrRuO_3$ in the ultrathin limit, Physical Review B **79**, 125444 (2009).

[44] M. Bjrck and G. Andersson, GenX: an extensible X-ray reflectivity refinement program utilizing differential evolution, Journal of Applied Crystallography **40**, 1174 (2007).

[45] B. M. Ludbrook, G. Dubuis, A.-H. Puichaud, B. J. Ruck, and S. Granville, Nucleation and annihilation of skyrmions in Mn_2CoAl observed through the topological Hall effect, Scientific Reports **7**, 1 (2017).

[46] M. Khalid, A. Setzer, M. Ziese, P. Esquinazi, D. Spemann, A. Pppl, and E. Goering, Ubiquity of ferromagnetic signals in common diamagnetic oxide crystals, Physical Review B **81**, 214414 (2010).